Lattice Boltzmann Simulation of Two-Fluid Model Equations

Krishnan Sankaranarayanan and Sankaran Sundaresan*

Department of Chemical Engineering, Princeton University, Princeton, New Jersey 08544

An implicit lattice Boltzmann equation to simulate the locally averaged flow behavior of disperse two-phase mixtures is presented. Using a multiscale expansion technique, it is shown that these equations reduce to the widely used two-fluid model for flows of such suspensions. The viability of the lattice Boltzmann approach is demonstrated through illustrative examples. The lattice Boltzmann scheme is easy to program and it parallelizes readily. It is suggested that this approach may serve as an attractive alternative to conventional approaches to solving the two-fluid model equations.

1. Introduction

Dispersed two-phase flows, such as those observed in fluidized beds and bubble columns, are prevalent in industrial practice.[1–4] Many of these flows are inherently unstable, and they manifest complex spatiotemporal structures. There is much interest in modeling and simulation of such flows in large process vessels, in order to understand the scale-up behavior and the influence of the flow patterns on various process characteristics such as heat and mass transfer, and selectivities and yields of chemical reactions. Dispersed two-phase flows are commonly analyzed through two-fluid model equations,[5–8] which treat the dispersed and continuous phases as interpenetrating continua, and locally averaged quantities such as the volume fractions, velocities, species concentrations, and temperatures of dispersed and continuous phases appear as dependent field variables. The averaging procedure leading to the two-fluid model equations introduces a number of terms, such as the interphase interaction force and the effective stresses in the dispersed and continuous phases, which require constitutive models. The two-fluid models are sometimes referred to as Euler−Euler models, to differentiate them from Euler−Lagrange approaches where the dispersed phase is tracked in a Lagrangian manner. Finite element and finite volume methods to solve the two-fluid model equations have been described extensively in the literature; for example, the open-domain software platform MFIX[9,10] is based on the finite volume method. Solution of these highly nonlinear discretized equations is challenging, as the equations for the dispersed and continuous phases are strongly coupled; while a fully coupled solver that solves iteratively all the discretized equations simultaneously is naturally indicated, it has largely remained prohibitively expensive and most of the computational studies employ a less efficient, sequential solver; for example see refs 9 and 10. Radically different approaches to solving such multiphase flow problems in a more efficient manner have the potential to expand the range of complex problems that one can solve with realistic resources; for example, the multiphase-particle-in-cell method described by Snider[11] has gained much traction in recent years. In the present paper, we present an alternate approach based on the lattice Boltzmann method (LBM) to solving the two-fluid model equations. Specifically, we propose the use of a modified lattice Boltzmann equation (LBE) with a Bhatnagar−Gross−Krook (BGK) collision term to indirectly simulate the two-fluid model equations. As the computations at each time step in the LBM are all "local", this approach can offer a considerable advantage over the conventional schemes such as the finite volume method.

The lattice Boltzmann method has been used extensively to solve single-phase flow problems; for example; see refs 12 and 13 It has also been applied to the detailed solution of a variety of two-phase problems.[14–30] For example, Ladd's pioneering work[14–17] established the framework to generate detailed solution of fluid-particle flows, where the motion of the fluid is tracked by LBM and the particle motion is followed by solving the Newton's equations; this approach has found widespread use in the literature to study model fluid−solid flow problems[18–25] and develop constitutive relations for the fluid−particle interaction force in two-fluid models for fluid−particle flows.[18–23] The LBM has also been applied to obtain detailed solution of the rise behavior of bubbly suspensions.[29,30] The present study differs from these studies in that we seek a lattice Boltzmann scheme to solve the two-fluid model equations. Flekkøy and Hermann[31] and Tan et al.[32] have used modified LBE to solve granular flow problems, while Wang and Wang[33] present modified LBE to solve a simple two-fluid model. The present analysis goes beyond these studies and develops the modified LBE to simulate the full two-fluid model equations that are commonly used to study dispersed two-phase flows.

The paper is organized as follows. We consider gas−particle flow as a model problem and describe in section 2 the kinetic theory based two-fluid model equations that are frequently used in the literature. The goal in this study is to develop a numerical scheme based on LBM to solve these two-fluid model equations. The theory behind the method is presented in section 3. The approach is validated through an example in section 4, and the main contributions of this study are summarized in section 5.

2. Two-Fluid Model for Gas−Particle Flows

Consider a dispersed two-phase system consisting of uniformly sized particles suspended in a continuous gas phase. The locally averaged equations of motion for the dispersed and continuous phases take the following form:[5–9]

$$\frac{\partial(\rho^{\mathrm{d}}\phi^{\mathrm{d}})}{\partial t} + \nabla\cdot(\rho^{\mathrm{d}}\phi^{\mathrm{d}}\mathbf{u}^{\mathrm{d}}) = 0 \tag{1}$$

$$\frac{\partial(\rho^{\mathrm{c}}\phi^{\mathrm{c}})}{\partial t} + \nabla\cdot[\rho^{\mathrm{c}}\phi^{\mathrm{c}}\mathbf{u}^{\mathrm{c}}] = 0 \tag{2}$$

$$\left[\frac{\partial(\rho^{\mathrm{d}}\phi^{\mathrm{d}}\mathbf{u}^{\mathrm{d}})}{\partial t} + \nabla\cdot(\rho^{\mathrm{d}}\phi^{\mathrm{d}}\mathbf{u}^{\mathrm{d}}\mathbf{u}^{\mathrm{d}})\right] = \nabla\cdot\boldsymbol{\pi}^{\mathrm{d}} + \phi^{\mathrm{d}}\nabla\cdot\boldsymbol{\pi}^{\mathrm{c}} + \mathbf{F} + \rho^{\mathrm{d}}\phi^{\mathrm{d}}\mathbf{g} \tag{3}$$

* To whom correspondence should be addressed. Tel.: (609) 258-4583. Fax: (609) 258-0211. E-mail: sundar@princeton.edu.

10.1021/ie800283b CCC: $40.75
Published on Web 07/02/2008

$$\left[\frac{\partial[\rho^c\phi^c\mathbf{u}^c]}{\partial t} + \nabla\cdot[\rho^c\phi^c\mathbf{u}^c\mathbf{u}^c]\right] = \phi^c\nabla\cdot\boldsymbol{\pi}^c - \mathbf{F} + \rho^c\phi^c\mathbf{g} \quad (4)$$

Here, $\phi^c = 1 - \phi^d$; ρ^c and ρ^d denote the densities of the continuous (gas) and dispersed (solid) phases; $\mathbf{u}^c$ and $\mathbf{u}^d$ are the local averages velocities of the two phases; $\boldsymbol{\pi}^c$ and $\boldsymbol{\pi}^d$ are the local average stresses; $\mathbf{F}$ denotes the interphase interaction force per unit volume; and $\mathbf{g}$ is the specific gravity force. Typically, the stress tensors are expressed as

$$\boldsymbol{\pi}^c = -p^c\mathbf{I} + \mu^c\left(\nabla\mathbf{u}^c + (\nabla\mathbf{u}^c)^T - \frac{2}{D}(\nabla\cdot\mathbf{u}^c)\mathbf{I}\right) \quad (5)$$

and

$$\boldsymbol{\pi}^d = -p^d\mathbf{I} + \mu_b^d(\nabla\cdot\mathbf{u}^d)\mathbf{I} + \mu^d\left(\nabla\mathbf{u}^d + (\nabla\mathbf{u}^d)^T - \frac{2}{D}(\nabla\cdot\mathbf{u}^d)\mathbf{I}\right) \quad (6)$$

Here, p^c and p^d denote the pressures; D denotes the dimension of the system ($D = 3$ for 3D); μ^c and μ^d are the effective (shear) viscosities of the two phases; μ_b^d is the bulk viscosity of the dispersed phase; and $\mathbf{I}$ is the identity tensor. (Typically, a bulk viscosity term is not included in the continuous phase stress, although it can readily be added in eq 5.) The continuous phase pressure p^c is either related to its density through an equation of state or treated as a separate variable for incompressible fluids. Here, we will allow the fluid to be compressible and assume that an equation of state is available. Constitutive models are needed for $\mathbf{F}$, μ^c, p^d, μ^d, and μ_b^d. In most gas−particle suspensions, the interphase interaction force is largely due to the drag and can be expressed as

$$\mathbf{F} = \beta(\mathbf{u}^c - \mathbf{u}^d) \quad (7)$$

where β is the friction coefficient. Several models have been described in the literature for β (e.g., see refs 18–22, 34–37), and all of them can be used in the scheme we present below. (In these models, the friction coefficient depends on the volume fraction of the discrete phase, the local relative velocity between the phases, the size of the discrete particles, and the physical properties of the continuous phase, and the interphase interaction force expression is highly nonlinear. Such nonlinearities can readily be handled in the methodology described in this paper.) We will present a sample closure relation for β later in section 4, when we validate the lattice Boltzmann scheme. In most gas−particle flows, the mass loading of particles is much larger than that of the gas, and the deviatoric stress in the continuous (gas) phase can often be neglected; but, retaining this term does not pose any special numerical challenges. We will allow for an empirically supplied μ^c in our analysis. The quantities appearing in the dispersed phase stress, namely, p^d, μ^d, and μ_b^d, are either closed phenomenologically or modeled through the kinetic theory of granular materials, which requires the solution of another equation (referred to as the pseudothermal or fluctuation energy balance) describing the evolution of the granular temperature associated with the random fluctuating motion of the discrete phase:[38–47]

$$\frac{\partial\left(\frac{D}{2}\rho^d\phi^dT^d\right)}{\partial t} + \nabla\cdot\left(\frac{D}{2}\rho^d\phi^dT^d\mathbf{u}^d\right) = -\nabla\cdot\mathbf{Q} + \boldsymbol{\pi}^d:\nabla\mathbf{u}^d + \Gamma_{slip} - J_{coll} - J_{vis} \quad (8)$$

Here, $T^d = \{1/D\}\langle\mathbf{C}\cdot\mathbf{C}\rangle$; $\mathbf{C}$ is the fluctuating velocity of the particle (discrete phase); Γ_{slip} is the rate of generation of fluctuation energy by gas−particle slip; J_{coll} and J_{vis} are the rates of dissipation of fluctuation energy by inelastic collisions between particles and viscous resistance of the gas; $\mathbf{Q}$ denotes the flux of pseudothermal energy is modeled as $Q = -\kappa\nabla T^d$, where κ is the pseudothermal conductivity. Constitutive models for p^d, μ^d, μ_b^d, κ, Γ_{slip}, J_{coll}, and J_{vis} in terms of dispersed phase diameter, density, coefficient of restitution, fluid properties, dispersed phase volume fraction, and the granular temperature have been described in the literature (for example, see ref 38) and need not be repeated here.

These equations must be supplemented with suitable initial and boundary conditions before they can be solved. Our goal is to establish a Lattice Boltzmann method to solve eqs 1–7, using either phenomenological closures for p^d, μ^d, and μ_b^d or eq 8 and associated closures. (Such options to choose the level of complexity of the model are routinely available in (the finite-volume based) open-domain package MFIX[9,10] and commercial software package such as Fluent.)

3. Theory

3.1. Continuum Boltzmann−BGK Model. Consider the following dimensionless Boltzmann−BGK equation (with modified collisional term) describing the evolution of the single-particle distribution function $f^\sigma(\mathbf{x},\boldsymbol{\xi},t)$, in the phase space $(\mathbf{x},\boldsymbol{\xi})$, where $\mathbf{x}$ and $\boldsymbol{\xi}$ are the position and microscopic velocity, respectively, for species σ:

$$\frac{\partial f^\sigma}{\partial t} + \boldsymbol{\xi}\cdot\nabla f^\sigma + \mathbf{g}^\sigma\cdot\nabla_{\boldsymbol{\xi}} f^\sigma = -\frac{1}{\tau^\sigma}(f^\sigma - f^{\sigma(0)}) + \frac{q^\sigma f^{\sigma(0)}}{D\rho^\sigma\phi^\sigma\theta^\sigma}\left(\frac{|\boldsymbol{\xi} - \mathbf{u}^\sigma|^2}{\theta^\sigma} - D\right) \quad (9)$$

Here $\mathbf{g}^\alpha$ is the acceleration due to the external force field acting on species σ (not necessarily conservative) and $\nabla_{\boldsymbol{\xi}}$ denotes the gradient in the velocity space. The right-hand side of eq 9 models the influence of collisions: the first term is the well-known BGK model for the collisions and the second term is newly added in the present study to tune the form of the (fluctuation) energy equation by carefully choosing the function q^α; as described later, the form of the second term and the choice of q^α ensure that the mass and momentum conservation equations are properly respected and the low order moments of the above equation yield the continuum two-fluid model that we set out to simulate. τ_α is the dimensionless relaxation time and $f^{\sigma(0)}$is the Maxwellian:

$$f^{\sigma(0)} = \frac{\rho^\sigma\phi^\sigma}{(2\pi\theta^\sigma)^{D/2}}e^{-|\boldsymbol{\xi} - \mathbf{u}^\sigma|^2/2\theta^\sigma} \quad (10)$$

The velocities $\mathbf{u}$ and $\boldsymbol{\xi}$ are normalized with respect to the constant reference sound speed $c_0 = \sqrt{k_BT_0/m_0}$, where k_B, T_0, and m_0 are the Boltzmann constant, a reference temperature, and the molecular mass of the particles, respectively. (The Boltzmann distribution in eq 10 is an equilibrium solution of eq 9.) $\theta^\alpha = m_0T^\alpha/m^\alpha T_0$ is the dimensionless temperature. Since, in general, $m^\alpha \neq m^{\bar\alpha}$ (where α and $\bar\alpha$ denote two different species), having $\theta^\alpha = \theta^{\bar\alpha}$ implies that $T^\alpha \neq T^{\bar\alpha}$, which is correct from a physical point of view as the granular temperature is not equal to the thermodynamic temperature. In the above equations, the characteristic length l and time t_0 satisfy $l/t_0 = c_0$, and the external acceleration is in the units of c_0/t_0. The first few moments of f^σ lead to

$$\rho^\sigma\phi^\sigma = \int f^\sigma\,d\xi \quad (11)$$

$$\rho^\sigma\phi^\sigma\mathbf{u}^\sigma = \int f^\sigma\xi\,d\xi \quad (12)$$

$$D\rho^\sigma\phi^\sigma\theta^\sigma = \int f^\sigma(\mathbf{u}^\sigma - \xi)^2\,d\xi \quad (13)$$

The quantity ϕ^σ is defined as follows. We first note that in our analysis $\sigma = 1,2$ and that one can readily find $\rho^\sigma\phi^\sigma$, $\sigma = 1, 2$ using eq 11. We now set the density of one of the two phases, say σ (typically that of the dispersed phase), to be constant and find its volume fraction using eq 11 and the prescribed density. The volume fraction of the second phase, say $\bar{\sigma}$ (typically that of the continuous phase), is then found by demanding that $\phi^{\bar{\sigma}} = 1 - \phi^\sigma$, which in turn allows determination of $\rho^{\bar{\sigma}}$ as $\rho^{\bar{\sigma}} = (\rho^{\bar{\sigma}}\phi^{\bar{\sigma}})/\phi^{\bar{\sigma}}$. We note the following identities, which will become useful later:

$$\int f^{\sigma(0)} c_i c_j c_k c_l \,\mathrm{d}\mathbf{c} = \frac{\rho^\sigma\phi^\sigma(\theta^\sigma)^2}{(2\pi)^{D/2}}\int \mathrm{e}^{-c^2/2} c_i c_j c_k c_l \,\mathrm{d}\mathbf{c} = \rho^\sigma\phi^\sigma(\theta^\sigma)^2(\delta_{ij}\delta_{kl} + \delta_{il}\delta_{jk} + \delta_{ik}\delta_{jl}) \tag{14}$$

$$\int f^{\sigma(0)} c^2 c_i c_j \,\mathrm{d}\mathbf{c} = \frac{\rho^\sigma\phi^\sigma(\theta^\sigma)^2}{(2\pi)^{D/2}}\int \mathrm{e}^{-c^2/2} c^2 c_i c_j \,\mathrm{d}\mathbf{c} = \rho^\sigma\phi^\sigma(\theta^\sigma)^2(D+2)\delta_{ij} \tag{15}$$

$$\int f^{\sigma(0)} c^4 \,\mathrm{d}\mathbf{c} = \frac{\phi^\sigma(\theta^\sigma)^2}{(2\pi)^{D/2}}\int \mathrm{e}^{-c^2/2} c^4 \,\mathrm{d}\mathbf{c}\,\rho^\sigma = \rho^\sigma\phi^\sigma(\theta^\sigma)^2(D+2)D \tag{16}$$

$$\int f^{\sigma(0)} c^4 c_i c_j \,\mathrm{d}\mathbf{c} = \frac{\rho^\sigma\phi^\sigma(\theta^\sigma)^3}{(2\pi)^{D/2}}\int \mathrm{e}^{-c^2/2} c^4 c_i c_j \,\mathrm{d}\mathbf{c} = \rho^\sigma\phi^\sigma(\theta^\sigma)^3(D+4)(D+2)\delta_{ij} \tag{17}$$

where $c = \xi - \mathbf{u}^\sigma$, $c^2 = \mathbf{c}\cdot\mathbf{c}$, and the subscripts denote components in the index notation.

By taking the various moments of eq 9, one can ready obtain the following mass, momentum, and fluctuation energy balance equations (expressed in index form):

$$\frac{\partial\rho^\sigma\phi^\sigma}{\partial t} + \frac{\partial\rho^\sigma\phi^\sigma u_i^\sigma}{\partial x_i} = 0 \tag{18}$$

$$\rho^\sigma\phi^\sigma\frac{\mathrm{d}u_i^\sigma}{\mathrm{d}t} + \frac{\partial P_{ij}^\sigma}{\partial x_j} = \rho^\sigma\phi^\sigma g_i^\sigma \tag{19}$$

$$\rho^\sigma\phi^\sigma\frac{\mathrm{d}\varepsilon^\sigma}{\mathrm{d}t} + P_{ij}^\sigma\frac{\partial u_i^\sigma}{\partial x_j} + \frac{1}{2}\frac{\partial S_i^\sigma}{\partial x_i} = q^\sigma \tag{20}$$

where $\varepsilon^\sigma = D\theta^\sigma/2$ is the fluctuation energy and $\mathrm{d}/\mathrm{d}t = \partial/\partial t + u_i^\sigma\,\partial/\partial x_i$. P_{ij}^σ and S_i^σ are the pressure (stress) and fluctuation energy flux, respectively.

$$P_{ij}^\sigma = \int f^\sigma c_i c_j \,\mathrm{d}\mathbf{c}, \quad S_i^\sigma = \int f^\sigma c^2 c_i \,\mathrm{d}\mathbf{c} \tag{21}$$

In the moment analysis leading to eqs 18–20, we have used the following properties:

$$\int \frac{q^\sigma f^{\sigma(0)}}{D\rho^\sigma\phi^\sigma\theta^\sigma}\left(\frac{|\xi - u^\sigma|^2}{\theta^\sigma} - D\right)\mathrm{d}\xi = \frac{q^\sigma}{D\rho^\sigma\phi^\sigma\theta^\sigma}\int f^{\sigma(0)}\left(\frac{|\xi - u^\sigma|^2}{\theta^\sigma} - D\right)\mathrm{d}\xi = \frac{q^\sigma}{D\rho^\sigma\phi^\sigma\theta^\sigma}(D\rho^\sigma\phi^\sigma\theta^\sigma - D\rho^\sigma\phi^\sigma\theta^\sigma) = 0$$

$$\int \frac{q^\sigma f^{\sigma(0)}}{D\rho^\sigma\phi^\sigma\theta^\sigma}\left(\frac{|\xi - u^\sigma|^2}{\theta^\sigma} - D\right)\xi\,\mathrm{d}\xi = 0$$

$$\int \frac{q^\sigma f^{\sigma(0)}}{D\rho^\sigma\phi^\sigma\theta^\sigma}\left(\frac{|\xi - u^\sigma|^2}{\theta^\sigma} - D\right)(\xi\cdot\xi)\,\mathrm{d}\xi = q^\sigma$$

Hydrodynamic equations can readily be derived using the Chapman−Enskog method of successive approximation. At zeroth order, $f^\sigma = f^{\sigma(0)}$; $P_{ij}^{\sigma(0)} = \rho^\sigma\phi^\sigma\theta^\sigma\delta_{ij}$; and $S_i^{\sigma(0)} = 0$. Equations 18–20 then become

$$\frac{\mathrm{d}(\rho^\sigma\phi^\sigma)}{\mathrm{d}t} = -\rho^\sigma\phi^\sigma\frac{\partial u_i^\sigma}{\partial x_i}$$

$$\rho^\sigma\phi^\sigma\frac{\mathrm{d}u_i^\sigma}{\mathrm{d}t} = -\frac{\partial(\rho^\sigma\phi^\sigma\theta^\sigma)}{\partial x_i} + \rho^\sigma\phi^\sigma g^\sigma$$

$$\frac{\mathrm{d}\theta^\sigma}{\mathrm{d}t} = -\frac{2\theta^\sigma}{D}\frac{\partial u_i^\sigma}{\partial x_i} + \frac{2}{D}\frac{q^\sigma}{\rho^\sigma\phi^\sigma} \tag{22}$$

At first order, substituting $f^\sigma = f^{\sigma(0)} + f^{\sigma(1)}$ into eq 9 and ignoring $f^{\sigma(1)}$ on the left-hand side (which is a standard simplification in the derivation of continuum equations from Boltzmann equation through perturbation expansion),[48] we arrive at

$$f^{\sigma(1)} \cong -\tau^\sigma\left(\frac{\partial}{\partial t} + \xi_i\frac{\partial}{\partial x_i} + g_i^\sigma\frac{\partial}{\partial\xi_i}\right)f^{\sigma(0)} + \tau^\sigma\frac{q^\sigma f^{\sigma(0)}}{D\rho^\sigma\phi^\sigma\theta^\sigma}\left(\frac{c^2}{\theta^\sigma} - D\right) \tag{23}$$

To evaluate the derivatives, we observe that the Maxwellian depends on t and $\mathbf{x}$ through the variables ϕ^σ, ρ^σ, $\mathbf{u}^\sigma$, and θ^σ, and use the following identities which can easily be verified from eq 10:

$$\frac{\partial f^{\sigma(0)}}{\partial(\rho^\sigma\phi^\sigma)} = \frac{f^{\sigma(0)}}{\rho^\sigma\phi^\sigma}, \quad \frac{\partial f^{\sigma(0)}}{\partial\theta^\sigma} = \left(\frac{c^2}{2\theta^\sigma} - \frac{D}{2}\right)\frac{f^{\sigma(0)}}{\theta^\sigma}, \quad \frac{\partial f^{\sigma(0)}}{\partial u_i^\sigma} = \frac{c_i f^{\sigma(0)}}{\theta_\sigma}, \quad \frac{\partial f^{\sigma(0)}}{\partial\xi_i} = -\frac{c_i f^{\sigma(0)}}{\theta^\sigma} \tag{24}$$

Equation 23 then becomes

$$f^{\sigma(1)} \cong -\frac{\tau^\sigma f^{\sigma(0)}}{\theta^\sigma}\left[\frac{\theta^\sigma}{\rho^\sigma\phi^\sigma}D(\rho^\sigma\phi^\sigma) + \left(\frac{c^2}{2\theta^\sigma} - \frac{D}{2}\right)\left(D(\theta^\sigma) + \frac{2}{D}\frac{q^\sigma}{\rho^\sigma\phi^\sigma}\right) + c_i D(u_i^\sigma) - g_i c_i\right] + \tau^\sigma\frac{q^\sigma f^{\sigma(0)}}{D\rho^\sigma\phi^\sigma\theta^\sigma}\left(\frac{c^2}{\theta^\sigma} - D\right) \tag{25}$$

where

$$D() = \frac{\partial}{\partial t} + \xi_i\frac{\partial}{\partial x_i} = \frac{\mathrm{d}}{\mathrm{d}t} + c_i\frac{\partial}{\partial x_i}$$

One then uses the zeroth-order solution (eq 22) to obtain

$$D(\rho^\sigma\phi^\sigma) = -\rho^\sigma\phi^\sigma\frac{\partial u_i^\sigma}{\partial x_i} + c_i\frac{\partial(\rho^\sigma\phi^\sigma)}{\partial x_i},$$

$$D(u_i^\sigma) = -\frac{1}{\rho^\sigma\phi^\sigma}\frac{\partial(\theta^\sigma\rho^\sigma\phi^\sigma)}{\partial x_i} + g_i^\sigma + c_j\frac{\partial u_i^\sigma}{\partial x_j},$$

$$D(\theta^\sigma) = -\frac{2\theta^\sigma}{D}\frac{\partial u_i^\sigma}{\partial x_i} + c_i\frac{\partial\theta^\sigma}{\partial x_i} \tag{26}$$

Combining eqs 25 and 26

$$f^{\sigma(1)} \cong -\frac{\tau^\sigma f^{\sigma(0)}}{\theta^\sigma}\left[\left(\frac{c^2}{2\theta^\sigma} - \frac{D+2}{2}\right)c_i\frac{\partial\theta^\sigma}{\partial x_i} + \left(c_i c_j - \frac{c^2}{D}\delta_{ij}\right)\frac{\partial u_i^\sigma}{\partial x_{ij}}\right] \tag{27}$$

Substituting this equation into eq 21), one obtains the first-order correction to the pressure tensor and fluctuation energy flux. The first term on the right-hand side of eq 27 is odd in c and therefore has no contribution to the pressure tensor; the second term is even in c and has no contribution to the energy flux. Using the identities presented earlier (eqs 14–17), one can

readily obtain the following for the pressure tensor and the energy flux:

$$P_{ij}^{\sigma(1)} = -\frac{\tau^\sigma}{\theta^\sigma}\frac{\partial u_k^\sigma}{\partial x_l}\int f^{\sigma(0)}\left(c_k c_l - \frac{c^2}{D}\delta_{kl}\right)c_i c_j \,\mathrm{d}\mathbf{c} = -2\tau^\sigma\theta^\sigma\rho^\sigma\phi^\sigma\left(\Lambda_{ij}^\sigma - \frac{\delta_{ij}}{D}\frac{\partial u_j^\sigma}{\partial x_j}\right) \quad (28)$$

$$S_i^{\sigma(1)} = -\frac{\tau^\sigma}{\theta^\sigma}\frac{\partial \theta^\sigma}{\partial x_j}\int f^{\sigma(0)}\left(\frac{c^2}{2\theta^\sigma} - \frac{D+2}{2}\right)c^2 c_i c_j \,\mathrm{d}\mathbf{c} = -(D+2)\tau^\sigma\theta^\sigma\rho^\sigma\phi^\sigma\frac{\partial\theta^\sigma}{\partial x_i} \quad (29)$$

where

$$\Lambda_{ij}^\sigma = \frac{1}{2}\left(\frac{\partial u_i^\sigma}{\partial x_j} + \frac{\partial u_j^\sigma}{\partial x_i}\right)$$

Substituting into eqs 18–20, and reverting back to vector notation, we obtain the following conservation equations (where we have set without loss of generality that $\sigma = 1$ is the dispersed phase and $\sigma = 2$ is the continuous phase):

$$\frac{\partial(\rho^\mathrm{d}\phi^\mathrm{d})}{\partial t} + \nabla\cdot(\rho^\mathrm{d}\phi^\mathrm{d}\mathbf{u}^\mathrm{d}) = 0 \quad (30)$$

$$\frac{\partial(\rho^\mathrm{c}\phi^\mathrm{c})}{\partial t} + \nabla\cdot(\rho^\mathrm{c}\phi^\mathrm{c}\mathbf{u}^\mathrm{c}) = 0 \quad (31)$$

$$\rho^\mathrm{d}\phi^\mathrm{d}\left[\frac{\partial\mathbf{u}^\mathrm{d}}{\partial t} + \mathbf{u}^\mathrm{d}\cdot\nabla\mathbf{u}^\mathrm{d}\right] = \nabla\cdot\left(-\rho^\mathrm{d}\phi^\mathrm{d}\theta^\mathrm{d}\mathbf{I} + \mu^\mathrm{d}\left(\nabla\mathbf{u}^\mathrm{d} + (\nabla\mathbf{u}^\mathrm{d})^T - 2\frac{\mathbf{I}}{D}\nabla\cdot\mathbf{u}^\mathrm{d}\right)\right) + \phi^\mathrm{d}\rho^\mathrm{d}\mathrm{g}^\mathrm{d} \quad (32)$$

$$\rho^\mathrm{c}\phi^\mathrm{c}\left[\frac{\partial\mathbf{u}^\mathrm{c}}{\partial t} + \mathbf{u}^\mathrm{c}\cdot\nabla\mathbf{u}^c\right] = \nabla\cdot(\phi^\mathrm{c}\boldsymbol{\pi}^\mathrm{c}) + \phi^\mathrm{c}\rho^\mathrm{c}\mathrm{g}^\mathrm{c} \quad (33)$$

$$\frac{D}{2}\rho^\mathrm{d}\phi^\mathrm{d}\left[\frac{\partial\theta^\mathrm{d}}{\partial t} + \mathbf{u}^\mathrm{d}\cdot\nabla\theta^\mathrm{d}\right] = -\nabla\cdot\mathbf{Q}^\mathrm{d} + \pi^\mathrm{d}\colon\nabla\mathbf{u}^\mathrm{d} + q^\mathrm{d} \quad (34)$$

$$\frac{D}{2}\rho^\mathrm{c}\phi^\mathrm{c}\left[\frac{\partial\theta^c}{\partial t} + \mathbf{u}^\mathrm{c}\cdot\nabla\theta^\mathrm{c}\right] = -\nabla\cdot\mathbf{Q}^c + \boldsymbol{\pi}^\mathrm{c}\colon\nabla\mathbf{u}^c + q^\mathrm{c} \quad (35)$$

where $\boldsymbol{\pi}^\mathrm{c}$ is as in eq 6 with

$$p^\mathrm{c} = -\rho^\mathrm{c}\theta^\mathrm{c};\quad \mu^\mathrm{c} = \rho^\mathrm{c}\tau^\mathrm{c}\theta^\mathrm{c};\quad \mu^\mathrm{d} = \rho^\mathrm{d}\phi^\mathrm{d}\tau^\mathrm{d}\theta^\mathrm{d};\quad Q^\sigma = -\frac{(D+2)}{2}\mu^\sigma\nabla\theta^\sigma,\quad \sigma = c,\ d \quad (36)$$

We define

$$\boldsymbol{g}^d = \boldsymbol{g} + \frac{1}{\phi^\mathrm{d}\rho^\mathrm{d}}[\mathbf{F} + \phi^\mathrm{d}\nabla\cdot\boldsymbol{\pi}^\mathrm{c} + \nabla\cdot((\phi^\mathrm{d}\rho^\mathrm{d}\theta^\mathrm{d} - p^\mathrm{d} + \mu_b^\mathrm{d}(\nabla\cdot\mathbf{u}^\mathrm{d}))\mathbf{I})] \quad (37)$$

$$\boldsymbol{g}^\mathrm{c} = \boldsymbol{g} - \frac{1}{\phi^\mathrm{c}\rho^\mathrm{c}}[F + \boldsymbol{\pi}^\mathrm{c}\cdot\nabla\phi^\mathrm{c}] \quad (38)$$

and

$$q^\mathrm{c} = 0;\quad q^\mathrm{d} = \Gamma_\mathrm{slip} - J_\mathrm{visc} - J_\mathrm{coll} \quad (39)$$

where $\mathbf{F}$, p^d, $\mu_\mathrm{b}^\mathrm{d}$, Γ_slip, J_visc, and J_coll (see section 2 for their definitions) are user-supplied functions, as in the two-fluid model outlined in section 2. Substituting the *definitions* specified in eqs 37–39 into eqs 32–35, we obtain

$$\rho^d\phi^\mathrm{d}\left[\frac{\partial\mathbf{u}^\mathrm{d}}{\partial t} + \mathbf{u}^\mathrm{d}\cdot\nabla\mathbf{u}^\mathrm{d}\right] = \phi^\mathrm{d}\nabla\cdot\boldsymbol{\pi}^\mathrm{c} + \nabla\cdot\boldsymbol{\pi}^\mathrm{d} + \mathbf{F} + \phi^\mathrm{d}\rho^\mathrm{d}\boldsymbol{g} \quad (40)$$

$$\rho_\mathrm{c}\phi^\mathrm{c}\left[\frac{\partial\mathbf{u}^\mathrm{c}}{\partial t} + \mathbf{u}^\mathrm{c}\cdot\nabla\mathbf{u}^\mathrm{c}\right] = \phi^\mathrm{c}\nabla\cdot\boldsymbol{\pi}^\mathrm{c} - \mathbf{F} + \phi^\mathrm{c}\rho^\mathrm{c}\boldsymbol{g} \quad (41)$$

$$\frac{D}{2}\rho^\mathrm{d}\phi^\mathrm{d}\left[\frac{\partial\theta^\mathrm{d}}{\partial t} + \mathbf{u}^\mathrm{d}\cdot\nabla\theta^\mathrm{d}\right] = -\nabla\cdot\mathbf{Q}^\mathrm{d} + \boldsymbol{\pi}^\mathrm{d}\colon\nabla\mathbf{u}^\mathrm{d} + \Gamma_\mathrm{slip} - J_\mathrm{coll} - J_\mathrm{vis} \quad (42)$$

$$\frac{D}{2}\rho^\mathrm{c}\phi^\mathrm{c}\left[\frac{\partial\theta^\mathrm{c}}{\partial t} + \mathbf{u}^c\cdot\nabla\theta^\mathrm{c}\right] = -\nabla\cdot\mathbf{Q}^\mathrm{c} + \boldsymbol{\pi}^\mathrm{c}\colon\nabla\mathbf{u}^\mathrm{c} \quad (43)$$

where $\boldsymbol{\pi}^\mathrm{d}$ is now as in eq 7. By choosing τ^d to be a function of ϕ^d (or any other variable), one can adjust the effective viscosity of the dispersed phase to match that of the two-fluid model in section 2. Note that the Prandtl number, Pr^σ, is a constant in the above model; although this restriction can be lifted with some modifications to the model, we do not pursue this further in the present paper. Comparing the continuum model deduced in this section with that presented in section 2, one can readily observe that all the equations are same with the exceptions that we now have a fluctuation energy equation for the continuous phase (eq 43) as well. This equation affects the continuity and momentum equations through the dependence of the density, pressure, and viscosity of the continuous phase on θ^c; however, the variation of θ^c can be made very small so that eq 43 is hardly relevant.

It is clear from the above analysis that the second term on the right-hand side of eq 9, the introduction of which is a key idea of the present work, has enabled eq 9 to behave like the two-fluid model we are interested in. The form of this term and the expressions for q^α (see eq 39) ensure that the low-order moments of eq 9 are the same as the mass and momentum conservation equations and the fluctuation energy balance of the two-fluid model.

3.2. Derivation of the Lattice Boltzmann−BGK Equations. Simulation of the continuous Boltzmann equations on the digital computers is done by first discretizing the equations. In this section, we outline the derivation of the *discrete* Boltzmann equation from the continuous Boltzmann−BGK model equations, which yield the lattice Boltzmann−BGK model (LBM-BGK) when applied to a regular grid.

We begin with eq 9 and approximate $\boldsymbol{g}^\sigma\cdot\nabla_\xi f^\sigma$ by $\boldsymbol{g}^\sigma\cdot\nabla_\xi f^{\sigma(0)}$, and absorb it into the Maxwellian to obtain[28,49]

$$\frac{\partial f^\sigma}{\partial t} + \xi\cdot\nabla_x f^\sigma = -\frac{f^\sigma - f^{\sigma(\mathrm{eq})}}{\tau^\sigma} + \frac{q^\sigma f^{\sigma(0)}}{D\rho^\sigma\phi^\sigma\theta^\sigma}\left(\frac{c^2}{\theta^\sigma} - D\right) \quad (44)$$

where

$$f^{\sigma(\mathrm{eq})} = f^{\sigma(0)}(\phi^\sigma\rho^\sigma, \mathbf{u}^\sigma + \boldsymbol{g}^\sigma\tau^\sigma, \theta^\sigma) \quad (45)$$

(This approximation is only valid for $|\boldsymbol{g}^\sigma\tau^\sigma|^2/2\theta^\sigma \ll 1$.) Integrating eq 44 over a time step δt[50,51]

$$f^\sigma(\mathbf{x} + \xi\delta t, \xi, t + \delta t) - f^\sigma(\mathbf{x}, \xi, t) = \int_t^{t+\delta t}\left[-\frac{f^\sigma - f^{\sigma(eq)}}{\tau^\sigma} + \frac{q^\sigma f^{\sigma(0)}}{D\rho^\sigma\phi^\sigma\theta^\sigma}\left(\frac{c^2}{\theta^\sigma} - D\right)\right]\mathrm{d}t \quad (46)$$

Different approximations can be used to simplify the right-hand side of eq 46. Choosing a trapezoidal rule

$$f^{\sigma}(\mathbf{x}+\xi\delta t,\xi,t+\delta t)-f^{\sigma}(\mathbf{x},\xi,t)= -\frac{\frac{1}{2}f^{\sigma}(\mathbf{x}+\xi\delta t,\xi,t+\delta t)-\frac{1}{2}f^{\sigma(\mathrm{eq})}(x+\xi\delta t,\xi,t+\delta t)}{\tau^{\sigma}}\delta t - \frac{+\frac{1}{2}f^{\sigma}(\mathbf{x},\xi,t)-\frac{1}{2}f^{\sigma(\mathrm{eq})}(\mathbf{x},\xi,t)}{\tau^{\sigma}}\delta t+ \frac{q^{\sigma}f^{\sigma(0)}(\mathbf{x}+\xi\delta t,\xi,t+\delta t)}{2D\rho^{\sigma}\phi^{\sigma}\theta^{\sigma}}\left(\frac{c^2}{\theta^{\sigma}}-D\right)\delta t+ \frac{q^{\sigma}f_q^{\alpha(0)}(\mathbf{x},\xi,t)}{2D\rho^{\sigma}\phi^{\sigma}\theta^{\sigma}}\left(\frac{c^2}{\theta^{\sigma}}-D\right)\delta t \quad (47)$$

Using Hermite discretization of the velocity space,[52] eq 47 can be written as

$$f_{\alpha}^{\sigma}(\mathbf{x}+\xi_{\alpha},t+1)-f_{\alpha}^{\sigma}(\mathbf{x},t)= -\left[\frac{1}{2}f_{\alpha}^{\sigma}(\mathbf{x}+\xi_{\alpha},t+1)+\frac{1}{2}f_{\alpha}^{\sigma}(\mathbf{x},t)-\frac{1}{2}f_{\alpha}^{\sigma(\mathrm{eq})}(\mathbf{x}+\xi_{\alpha},t+1)-\frac{1}{2}f_{\alpha}^{\sigma(\mathrm{eq})}(\mathbf{x},t)\right]\Big/\tau^{\sigma}+\frac{q^{\sigma}f_{\alpha}^{\sigma(0)}(\mathbf{x}+\xi_{\alpha},t+1)}{2D\rho^{\sigma}\phi^{\sigma}\theta^{\sigma}}\left(\frac{c^2}{\theta^{\sigma}}-D\right)+ \frac{q^{\sigma}f_{\alpha}^{\sigma(0)}(\mathbf{x},t)}{2D\rho^{\sigma}\phi^{\sigma}\theta^{\sigma}}\left(\frac{c^2}{\theta^{\sigma}}-D\right) \quad (48)$$

where time has been rescaled to make $\delta t = 1$. Here, f_{α}^{σ} are related to $f^{\sigma}(\mathbf{x},\xi,t)$ through

$$f_{\alpha}^{\sigma}(\mathbf{x},t)=\frac{\varpi_{\alpha}}{\omega(\boldsymbol{\xi}_{\alpha})}f^{\sigma}(\mathbf{x},\xi_{\alpha},t);\quad \omega(\boldsymbol{\xi})=\left(\frac{1}{2\pi}\right)^{D/2}\mathrm{e}^{-\frac{\boldsymbol{\xi}\cdot\boldsymbol{\xi}}{2}} \quad (49)$$

Here, $\omega(\xi)$ is the chosen weight function; $\boldsymbol{\xi}_{\alpha}$ are the abscissas of the quadrature in the velocity space:[50–52]

$$\xi_{\alpha}=\begin{cases}(0,0) & \alpha=0\\ (\cos\phi_{\alpha},\sin\phi_{\alpha})\sqrt{3},\ \phi_{\alpha}=(\alpha-1)\pi/2 & \alpha=1-4\\ (\cos\phi_{\alpha},\sin\phi_{\alpha})\sqrt{6},\ \phi_{\alpha}=(\alpha-5)\pi/2+\pi/4 & \alpha=5-8\end{cases} \quad (50)$$

in two dimensions, and

$$\xi_{\alpha}=\begin{cases}(0,0,0) & \alpha=0\\ (\pm\sqrt{3},0,0),(0,\pm\sqrt{3},0),(0,0,\pm\sqrt{3}) & \alpha=1-6\\ (\pm\sqrt{3},\pm\sqrt{3},\pm\sqrt{3}) & \alpha=7-14\end{cases} \quad (51)$$

in three dimensions. ϖ_{α} are the quadrature weights:[50–52]

$$\varpi_{\alpha}(\text{in } 2D)=\begin{cases}4/9, & \alpha=0\\ 1/9, & \alpha=1-4\\ 1/36, & \alpha=5-8\end{cases}$$

$$\varpi_{\alpha}(\text{in } 3D)=\begin{cases}2/9, & \alpha=0\\ 1/9, & \alpha=1-6\\ 1/72, & \alpha=7-14\end{cases} \quad (52)$$

Consistent with this discretization of the velocity space, the physical space assumes the form of a square (cubic) lattice in 2D (3D) with a lattice spacing of $\sqrt{3}$. Further details of this derivation can be found in refs 50–52.

The various moments are now related to f_{α}^{σ} according to

$$\rho^{\sigma}\phi^{\sigma}=\sum_{\alpha}f_{\alpha}^{\sigma} \quad (53)$$

$$\rho^{\sigma}\phi^{\sigma}\mathbf{u}^{\sigma}=\sum_{\alpha}f_{\alpha}^{\sigma}\boldsymbol{\xi}_{\alpha} \quad (54)$$

$$D\rho^{\sigma}\phi^{\sigma}\theta^{\sigma}=\sum_{\alpha}f_{\alpha}^{\sigma}(\mathbf{u}^{\sigma}-\boldsymbol{\xi}_{\alpha})^2 \quad (55)$$

To summarize the theory section, we showed in section 3.1 the equivalence between the continuum Boltzmann−BGK model and the two-fluid model. In section, we then discretized the Boltzmann equation and obtained the LBM-BGK equations. It is straightforward to show through Taylor series expansion of the discrete equations and use of the Chapman−Enskog ansatz that simulation of the LBM-BGK equations is also equivalent to solving the two-fluid model equations, and so the details are not presented here.

3.3. Stability Analysis of the Lattice Boltzmann−BGK Equations. In section 3.2 we presented an implicit numerical scheme to simulate the two-fluid model equations. When using an *explicit* LBM[12] to simulate single phase flows (as an approximation for the Navier−Stokes equations), one of the limitations is the numerical stability of the scheme[53,54] imposed by the Courant−Friedrichs−Lewy condition.[55] Since the success and applicability of numerical schemes depend in part on the numerical stability thereof, it is important to examine the issue of numerical instability for the implicit scheme proposed in section 3.2. Equation 47) can be rearranged as

$$f_{\alpha}^{\sigma}(\mathbf{x}+\boldsymbol{\xi}_{\alpha},t+1)=\frac{\tau^{\sigma}-\frac{1}{2}}{\tau^{\sigma}+\frac{1}{2}}f_{\alpha}^{\sigma}(\mathbf{x},t)+\frac{\frac{1}{2}}{\tau^{\sigma}+\frac{1}{2}}(f_{\alpha}^{\sigma(0)}(\mathbf{x}+\xi_{\alpha},t+1)+f_{\alpha}^{\sigma(0)}(\mathbf{x},t))+\frac{\frac{1}{2}\tau^{\sigma}}{\tau^{\sigma}+\frac{1}{2}}\frac{q^{\sigma}}{D\rho^{\sigma}\phi^{\sigma}\theta^{\sigma}}(f_{\alpha}^{\sigma(0)}(\mathbf{x}+\boldsymbol{\xi}_{\alpha},t+1)+f_{\alpha}^{\sigma(0)}(\mathbf{x},t))\left(\frac{c^2}{\theta^{\sigma}}-D\right) \quad (56)$$

From this, one can deduce that the numerical scheme is stable for all $\tau^{\sigma} > 0$, as that would ensure that $|(\tau^{\sigma}-{}^1/_2)/(\tau^{\sigma}+{}^1/_2)| < 1$. The implicit scheme thus removes any restriction on the relaxation time τ^{σ}, thus allowing for a larger parameter space which can be simulated economically.[29]

4. Test Example

a. Methodology. It is important to keep in mind that the LBM simulations are done in the so-called *lattice units*. Thus, in order to compare the LBM results with those for a physical problem, it is important to translate the LBM results into a suitable dimensionless form (by combining the quantities in lattice units). One can then compare the LBM results with those of a physical problem where the results of the physical problem are also scaled in terms of identical dimensionless groups. Thus, the first task is to analyze first the physical situation at hand and identify the important dimensionless groups. It is worth reemphasizing that this is necessary as the lattice Boltzmann method uses lattice units, and the LBM problem needs to be set up in lattice units, and will yield results in lattice units, which must then be translated back to physical units via dimensionless groups.

The second task is to determine the grid resolution which is necessary for the problem, the upper bound of which is determined by the computer hardware. A key feature here is, though, that the selection of the grid resolution, or number of computational grids, essentially also fixes one of the lattice

length scale which will be used in the translation of the lattice results. We will illustrate this in this section.

The third task involves the initialization of the f_α^σ. The simplest way of initializing the problem is to assign the equilibrium values to these variables.

The fourth task in the simulation is to allow the evolution of the system according to eq 48. Once the f_α^σ are known as functions of time, we can readily find the hydrodynamic quantities through eq 53–55.

The approach can be summarized as follows:

1. Determine dimensionless groups which are to be matched.
2. Determine grid resolution and values of the parameters in the simulation.
3. Determine the initial values of $\phi^\sigma\rho^\sigma$, u^σ, θ^σ and use these values to initialize f_α^σ using $f_\alpha^\sigma = f_\alpha^{\sigma(0)}(\phi^\sigma\rho^\sigma,u^\sigma,\theta^\sigma)$. This sets the values at $t = 0$.
4. Increase time by one time step and compute the values of f_α^σ using eq 48.
5. Quantities of hydrodynamic interest, such as $\phi^\sigma\rho^\sigma,u^\sigma,\theta^\sigma$ etc can be computed as successive moments in the velocity space of f_α^σ using eqs 53–55.
6. Go back to step 4 and repeat until simulation has ended.

In order to validate the proposed computational scheme, we reproduce here some of the results presented earlier by Glasser et al.[56] for gas−particle flows. These authors first examined the linear stability of the uniformly fluidized state using the two-fluid model, supplemented with phenomenological constitutive equations, and then examined the fate of a linearly unstable bed through transient integration in one- and two-dimensional periodic domains. We will demonstrate that nearly identical results can be generated through the current LBM approach as well. Glasser et al.[56] assumed that

$$\mathbf{F} = \beta(\phi^{\mathrm{d}})(\mathbf{u}^{\mathrm{c}} - \mathbf{u}^{\mathrm{d}}); \quad \beta(\phi^{\mathrm{d}}) = \frac{(\rho^{\mathrm{d}} - \rho^{\mathrm{c}})g\phi^{\mathrm{d}}}{v_t(1-\phi^{\mathrm{d}})^{n-2}} \tag{54}$$

$$p^{\mathrm{d}} = C_1(\phi^{\mathrm{d}})^3 \exp\left[\frac{r\phi^{\mathrm{d}}}{\phi_{\mathrm{p}}^{\mathrm{d}} - \phi^{\mathrm{d}}}\right]; \quad \mu^{\mathrm{d}} = \frac{A\phi^{\mathrm{d}}}{1 - (\phi^{\mathrm{d}}/\phi_{\mathrm{p}}^{\mathrm{d}})^{\frac{1}{3}}} \tag{55}$$

Here, v_t, $\phi_{\mathrm{p}}^{\mathrm{d}}$, C_1, n, r, and A are model parameters. These authors made the two-fluid model equations dimensionless using ρ^{d}, v_t, and $L = \{Av_t\}/\{\rho^{\mathrm{d}}g\}$ as characteristic density, velocity, and length, respectively. This led to the following dimensionless groups: $\delta = \rho_{\mathrm{c}}/\rho_{\mathrm{d}}$, $\gamma = \mu^{\mathrm{c}}/A$, $\alpha = \{C_1\}/\{\rho^{\mathrm{d}}v_t^2\}$, and $\Omega = (\{\rho^{\mathrm{d}}v_t^3\}/\{Ag\})^{1/2}$. (These authors did not consider the fluctuation energy balance equation in their analysis.) Using this model, they determined the growth rate of one-dimensional disturbances (that have no horizontal structure) imposed on a uniformly fluidized state of specified particle volume fraction for various wavenumbers. The solid line in Figure 1a illustrates the dimensionless growth rate as a function of the vertical wavenumber for a homogeneous fluidized bed with $\phi^{\mathrm{d}} = \phi_0 = 0.57$ (see their Table 1 and Figure 1 for parameter values).

We set out to reproduce these results using the LBM approach described in this paper. To make a correspondence with Glasser et al.[56] results, the dimensionless groups mentioned above must be matched in our LBM simulations. L is the important lengthscale and the matching occurs through the wavenumber $k_y = (2\pi L)/(\sqrt{3}L_{\mathrm{B}})$, where L_{B} is the number of computational nodes in the LBM simulation. The choice of L_{B} is not unique, and one can match all groups with different L_{B} values (or equivalently, LBM simulations at different spatial resolutions). The analysis by Glasser et al.[56] was done in periodic domains which can readily be implemented in the lattice Botzmann simulations by demanding that the f_α^σ be periodic. As the LBM approach does not permit direct observation of the evolution of the moments, we employed the LBM approach to follow the evolution of a disturbance imposed on the uniformly fluidized bed and determined how the amplitude of the disturbance evolved with time; from this, we extracted the growth rate. The LBM simulations were done in two-dimensional periodic domains, just as in Glasser et al.[56] To evaluate the one-dimensional growth rate, the lateral width of the periodic domain was chosen to be small (so that the growth of two-dimensional structures are suppressed). Specifically, the simulations were performed using $4 \times L_{\mathrm{B}}$ grids. The dimensionless wavenumber (in Glasser et al.[56]) corresponding to such a simulation would then be $k_y = 2\pi L/\sqrt{3}L_{\mathrm{B}}$; thus, by varying L_{B}, one can find the growth rates for various wavenumbers. (Using such an approach,

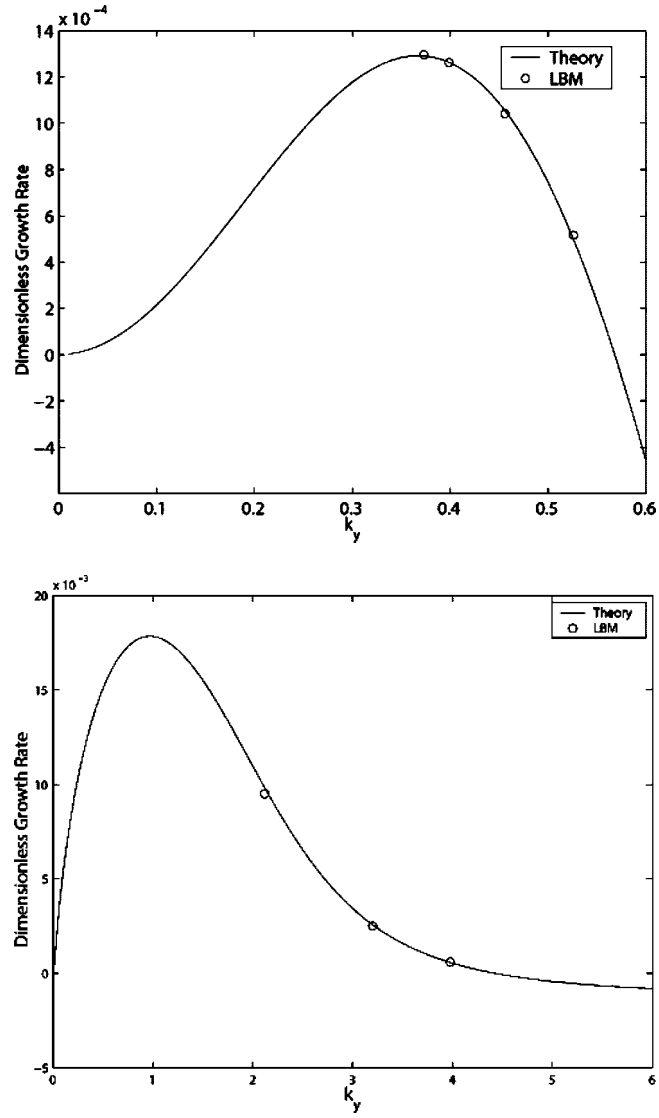

Figure 1. (a, top) Dimensionless growth rate of a one-dimensional disturbance vs dimensionless vertical wavenumber k_y. Comparison of LBM and linear stability (Glasser et al.[56]) for $\phi_0 = 0.57$. The values of the various dimensionless groups are $\alpha = 0.000\,242$, $\gamma = 0.000\,363$, $\delta = 0.000\,590\,909$, $\Omega = 113.481$. The solid line indicates the results from linear stability analysis of the two-fluid model. The circles indicate results extracted from LBM simulations with 4×855 computational nodes. (b, bottom) Dimensionless growth rate of a one-dimensional disturbance vs dimensionless vertical wavenumber k_y. Comparison of LBM and linear stability analysis results for $\phi_0 = 0.05$. The values of the various dimensionless groups are as in Figure 1a. The solid line indicates the results from linear stability analysis of the two-fluid model. The circles indicate results extracted from LBM simulations with 4×855 computational nodes.

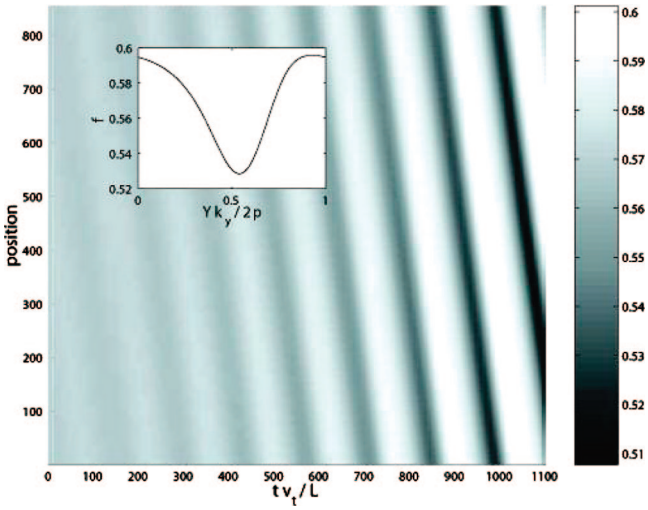

Figure 2. Grayscale plot of spatio-temporal evolution of voidage field. LBM simulations with 4 × 855 computational nodes. $\phi_0 = 0.57$. The values of the various dimensionless groups are as in Figure 1a. $k_y = 0.37$. Note that darker regions correspond to lower particle volume fractions.

one can find only the growth rates that lie to the right of the maximum in Figure 1a.) The circles in Figure 1 are obtained through the LBM simulations; the agreement is very good, validating the LBM approach. (See Appendix for an additional discussion as to why LBM simulations were done only for points to the right side of the peak in this figure.) Figure 1b is obtained for a different homogeneously fluidized bed with $\phi^d = \phi_0 = 0.05$; once again, the agreement is good, confirming that the LBM approach is applicable for both dilute and dense fluidized suspensions.

Figure 2 shows a grayscale plot of the results of an LBM simulation which was used to compute the growth rate shown in Figure 1a (at $k_y = 0.37$). The abscissa and the ordinate denote dimensionless time and spatial location, respectively. Different grades of gray correspond to different particle volume fractions; as seen in this figure, the base state ($\phi^d = \phi_0 = 0.57$) is unstable and gives way to a one-dimensional traveling wave (a snapshot of which is illustrated in the inset). The amplitude of this wave grows exponentially at early times and then reaches a fully developed state. This is fully consistent with the findings of Glasser et al.[56]

Figure 3 illustrates the development of inhomogeneous structure in a square box, where two-dimensional structures can grow (as the periodic box is wide in lateral dimensions as well). The homogeneously fluidized state was initially perturbed with a small disturbance (having only vertical structure) and the evolution was followed via LBM. It is clear from this figure that the evolution proceeds initially as a 1-D traveling wave and that after the amplitude of this 1-D wave has become sufficiently large, two-dimensional structures emerge (leading to a bubble-like void). This is precisely the same evolution path that Glasser et al.[56] describe in detail. (The grayscale in the present study is opposite of that of Glasser et al.,[56] with dark region now representing the void.)

Figure 4 shows the evolution of a two-dimensional structure in a dilute fluidized bed, where one can see the evolution of a particle-rich region (cluster/streamer), which is also well-known.[38,57]

5. Summary

In this study, we have presented a lattice Boltzmann scheme to solve the two-fluid model equations, which can be used as an alternative to the conventional finite element or finite volume

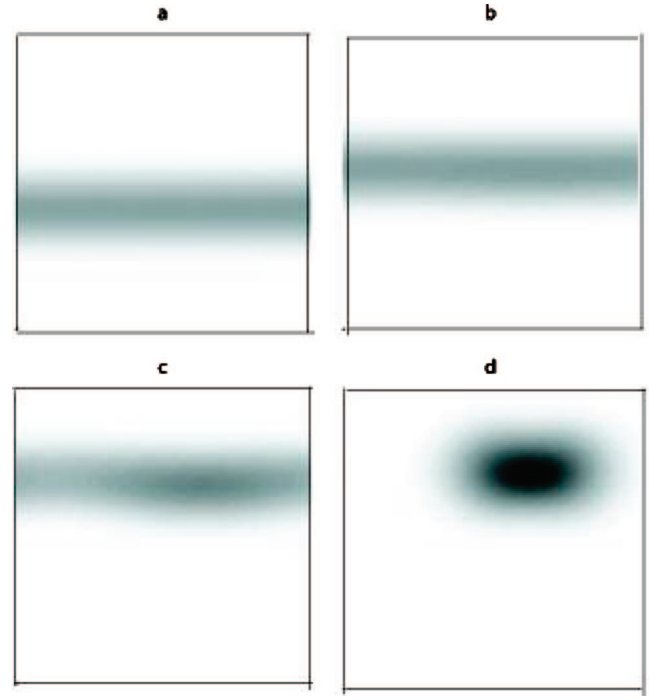

Figure 3. Grayscale plot of spatio-temporal evolution of voidage field leading to a 2-D bubble-like void. LBM simulations with 64 × 64 computational nodes. $\phi_0 = 0.57$. The values of the various dimensionless groups are as in Figure 1a. $k_x = k_y = 0.1$. Note that darker regions correspond to lower particle volume fractions. (a) $tv_t/L = 2524$, (b) $tv_t/L = 2602$, (c) $tv_t/L = 2681$, (d) $tv_t/L = 2760$.

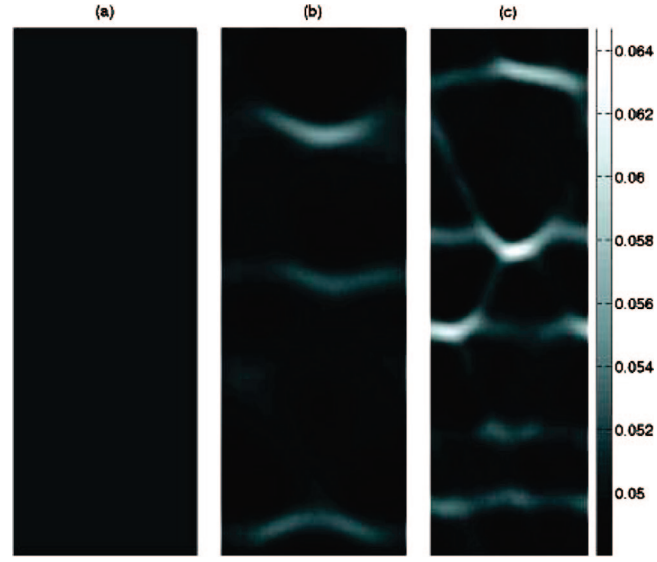

Figure 4. Grayscale plot of spatio-temporal evolution of voidage field leading to 2-D clusters and streamers. LBM simulations with 100 × 100 computational nodes. $\phi_0 = 0.05$, The values of the various dimensionless groups are as in Figure 1a. $k_x = k_y = 0.1$. Note that darker regions correspond to lower particle volume fractions. (a) $tv_t/L = 25$, (b) $tv_t/L = 6200$, (c) $tv_t/L = 7437$.

approaches. We have demonstrated that the spatiotemporal structures that are known to occur in both dilute and dense fluidized beds can be captured through the LBM approach proposed here. The LBM approach described in this study is extremely simple to code and it parallelizes easily as all the computations are local. Although the methodology was developed to include the kinetic theory based constitutive models, the illustrative example considered a simplified two-fluid model

with phenomenological closures, so that direct comparisons can be made with previously published results.

Further work building on this study should strive to (b) implement the kinetic theory closures and (b) evaluate the potential advantages of the LBM approach in simulating more complicated disperse flows in complex geometries. To do the latter, one must first develop and test schemes to implement the boundary conditions are solid walls; implementing no-slip or free-slip type boundary conditions are readily done using the bounce-back and reflect schemes, which have been well tested in single-phase flows, while the more commonly used partial slip boundary conditions for the discrete phase requires new schemes and validation. A head-to-head comparison of the LBM approach with the more conventional CFD approaches must also be done to expose the strengths and weaknesses of the LBM approach; only then can one ascertain whether or not the methodology proposed in this study is more desirable than the conventional approaches.

Acknowledgment

The authors are indebted to Dr. Xiaowen Shan for sharing his notes on the derivation of the Navier−Stokes and energy equations from the continuum and discrete Boltzmann equation. One of us (S.S.) is delighted to submit this paper for the special issue honoring Professor Arvind Varma, who has been a dear and respected friend for a long time.

Appendix

The solid line in Figure 1a was obtained by a formal linear stability analysis which allows one to focus on disturbance of a particular wavenumber. Higher harmonics of this chosen wavenumber disturbance do not enter in the analysis, and the growth rate of the disturbance pertains to that specific wavenumber. As a result, one can investigate the outcome of disturbance of various wavenumbers over the entire spectrum $(0,\infty)$ one at a time.

In contrast, in the present study, we have performed transient integration of the lattice Boltzmann equations for various chosen periodic box sizes (equivalent to wavelength), starting from a slightly perturbed homogeneous state. In such a numerical approach where one solves a discretized system of equations, one observes the evolution of not only the disturbance whose wavelength is the same as the box size, but also several higher harmonics. Thus, for example, if one considers an one-dimensional periodic domain of length L discretized using $2N + 1$ grids, then resulting transient solution will include features with wavelengths L, $L/2$, $L/3$,..., L/N. When the box size is L is such that the wavenumber $2\pi/L$ is to the right of the peak in Figure 1a, then the fastest growth rate will correspond to a wave with wavelength L. However, when the box size L is sufficiently large that the wavenumber $2\pi/L$ is to the left of the peak in Figure 1a, the fastest growing wave may no longer be the one with wavelength L. In our simulations, we specifically sought the fastest growing mode. It is generally hard to extract the growth rates of slower linear modes accurately from such a simulation (as a result of nonlinear effects). Consequently, we carried out simulations only for box sizes smaller than that corresponding to the peak growth rate in Figure 1a.

Literature Cited

(1) Kunii, D.; Levenspiel, O. *Fluidization Engineering*; 2nd ed.; Butterworth-Heinemann: Boston, 1991.

(2) Kastanek, F.; Zahradnik, J.; Kratochvil, J.; Cermak, J. *Chemical Reactors for Gas-Liquid Systems*; Ellis-Horwood: New York, 1993.

(3) Deckwer, W. D. *Bubble Column Reactors*; translated by Cottrel, V., Field, R. W., Eds.; Wiley: New York, 1992.

(4) van Baten, J. M.; Krishna, R. Modeling sieve tray hydraulics using computational fluid dynamics. *Chem. Eng. J.* **2000**, *77*, 143.

(5) Gidaspow D. *Multiphase Flow and Fluidization*; Academic Press: San Diego, 1994.

(6) Jackson R. *The dynamics of fluidized particles*; Cambridge University Press: London, 2000.

(7) Anderson, T. B.; Jackson, R. Fluid mechanical description of fluidized beds. *Ind. Eng. Chem. Fundam.* **1967**, *6*, 527.

(8) Jackson, R. Locally averaged equations of motion for a mixture of identical spherical particles and a Newtonian fluid. *Chem. Eng. Sci.* **1997**, *52*, 2457.

(9) Syamlal, M.; Rogers, W.; O'Brien, T. J. *MFIX Documentation*; U.S. Department of Energy, Federal Energy Technology Center: Morgantown, WV, 1993.

(10) Syamlal, M. *MFIX Documentation: Numerical Techniques*; DOE/MC-31346-5824. NTIS/DE98002029, 1998. Also see www.mfix.org.

(11) Snider, D. M. An incompressible, three-dimensional multiphase particle-in-cell model for dense particle flows. *J. Comput. Phys.* **2001**, *170*, 523.

(12) Chen, S.; Doolen, G. Lattice Boltzmann method for fluid flows. *Annu. Rev. Fluid Mech.* **1998**, *30*, 329.

(13) Eggels, J. G. M.; Somers, J. A. Numerical simulation of free convective flow using the lattice-Boltzmann scheme. *Int. J. Heat Fluid Flow* **1995**, *16*, 357.

(14) Ladd, A. J. C. Numerical simulations of particulate suspensions via a discretized Boltzmann equation. Part 1. Theoretical foundation. *J. Fluid Mech.* **1994**, *271*, 285.

(15) Ladd, A. J. C. Numerical simulations of particulate suspensions via a discretized Boltzmann equation. Part 2. Numerical Results. *J. Fluid Mech.* **1994**, *271*, 311.

(16) Ladd, A. J. C.; Verberg, R. Lattice-Boltzmann simulations of particle-uid suspensions. *J. Stat. Phys.* **2001**, *104*, 1191.

(17) Nguyen, N.-Q.; Ladd, A. J. C. Lubrication corrections for lattice-Boltzmann simulations of particle suspensions. *Phys. Rev. E* **2002**, *66*, 046708.

(18) Hill, R. J.; Koch, D. L.; Ladd, A. J. C. The first effects of fluid inertia on flows in ordered and random arrays of spheres. *J. Fluid Mech.* **2001**, *448*, 213.

(19) Hill, R. J.; Koch, D. L.; Ladd, A. J. C. Moderate-Reynolds-number flows in ordered and random arrays of spheres. *J. Fluid Mech.* **2001**, *448*, 243.

(20) van der Hoef, M. A.; Beetstra, R.; Kuipers, J. A. M. Lattice-Boltzmann simulations of low-Reynolds-number flow past mono- and bidisperse arrays of spheres. *J. Fluid Mech.* **2005**, *528*, 233.

(21) Beetstra, R.; van der Hoef, M. A.; Kuipers, J. A. M. Drag force of intermediate Reynolds number flows past mono- and bidisperse arrays of spheres. *AIChE J.* **2007**, *53*, 489.

(22) Wylie, J. J.; Koch, D. L. Rheology of suspensions with high particle inertia and moderate fluid inertia. *J. Fluid Mech.* **2003**, *480*, 95.

(23) Kandhai, D.; Derksen, J. J.; Van den Akker, H. E. A. Interphase drag coefficients in gas-solid flows. *AIChE J.* **1998**, *49*, 1060.

(24) Derksen, J. J.; Sundaresan, S. DNS of dense suspensions: Wave instabilities in liquid-fluidized beds. *J. Fluid Mech.* **2007**, *587*, 303.

(25) Aidun, C. K.; Lu, Y.; Ding, E. J. Direct analysis of particle suspensions with inertia using the discrete Boltzmann equation. *J. Fluid Mech.* **1998**, *373*, 287.

(26) Shan, X. Simulation of Rayleigh-Benard convection using a lattice Boltzmann method. *Phys. Rev. E* **1997**, *55*, 2780.

(27) Palmer, B. J.; Rector, D. R. Lattice Boltzmann algorithm for simulating thermal two-phase flow. *Phys. Rev. E* **2000**, *61*, 5295.

(28) Shan, X.; Chen, H. Lattice Boltzmann model for simulating flows with multiple phases and components. *Phys. Rev. E* **1993**, *47*, 1815.

(29) Sankaranarayanan, K.; Shan, X.; Kevrekidis, I. G.; Sundaresan, S. Analysis of drag and virtual mass forces in bubbly suspensions using an implicit formulation of the lattice Boltzmann method. *J. Fluid Mech.* **2002**, *452*, 61.

(30) Sankaranarayanan, K.; Sundaresan, S. Lift Force in Bubbly Suspensions. *Chem. Eng. Sci.* **2002**, *57*, 3521.

(31) Flekkoy, E. G.; Hermann, H. J. Lattice Boltzmann models for complex flows. *Physica A* **1993**, *199*, 1.

(32) Tan, M.-L.; Qian, Y. H.; Goldhirsch, I.; Orszag, S. A. Lattice-BGK approach to simulating granular flows. *J. Stat. Phys.* **1995**, *81*, 87.

(33) Wang, T.; Wang, J. Two-fluid model based on the lattice Boltzmann equation. *Phys. Rev. E* **2005**, *71*, 045301.

(34) Wen, C. Y.; Yu, Y. H. Mechanics of fluidization. *Chem. Eng. Prog. Symp. Ser.* **1966**, *62*, 100.

(35) Richardson, J. F.; Zaki, W. N. Sedimentation and fluidization: Part I. *Trans. Inst. Chem. Eng.* **1954**, *32*, 35.

(36) Li, J.; Kuipers, J. A. M. Gas-particle interactions in dense gas-fluidized beds. *Chem. Eng. Sci.* **2003**, *58*, 711.

(37) Benyahia, S.; Syamlal, M.; O'Brien, T. J. Extension of Hill-Koch-Ladd drag correlation over all ranges of Reynolds number and solid volume fraction. *Powder Technol.* **2006**, *162*, 166.

(38) Agrawal, K.; Loezos, P. N.; Syamlal, M.; Sundaresan, S. The Role of meso-scale structures in rapid gas-solid flows. *J. Fluid Mech.* **2001**, *445*, 151.

(39) Gidaspow, D.; Jung, J.; Singh, R. J. Hydrodynamics of fluidization using kinetic theory: An emerging paradigm. 2002 Fluor-Daniel Lecture. *Powder Technol.* **2004**, *148*, 123.

(40) Koch, D. L.; Sangani, A. S. Particle pressure and marginal stability limits for a homogeneous monodisperse gas fluidized bed: kinetic theory and numerical simulations. *J. Fluid Mech.* **1999**, *400*, 229.

(41) Ding, J.; Gidaspow, D. A Bubbling fluidization model using kinetic-theory of granular flow. *AIChE J.* **1990**, *36*, 523.

(42) Benyahia, S.; Arastoopour, H.; Knowlton, T. M. Simulation of particles and gas flow behavior in the riser section of a circulating fluidized bed using the kinetic theory approach for the particulate phase. *Powder Technol.* **2000**, *112*, 24.

(43) Goldschmidt, M. J. V.; Kuipers, J. A. M.; van Swaaij, W. P. M. Hydrodynamic modeling of dense gas-fluidized beds using the kinetic theory of granular flow: Effect of restitution coefficient on bed dynamics. *Chem. Eng. Sci.* **2001**, *56*, 571.

(44) Neri, A.; Gidaspow, D. Riser hydrodynamics: Simulation using kinetic theory. *AIChE J.* **2000**, *46*, 52.

(45) Lun, C. K. K.; Savage, S. B.; Jeffrey, D. J.; Chepurniy, N. Kinetic theories of granular flows: inelastic particles in Couette flow and slightly inelastic particles in a general flow field. *J. Fluid Mech.* **1984**, *140*, 223.

(46) Sinclair, J. L.; Jackson, R. Gas-particle flow in a vertical pipe with particle-particle interaction. *AIChE J.* **1989**, *35*, 1473.

(47) Pita, J. A.; Sundaresan, S. Gas-solid flow in vertical tubes. *AIChE J.* **1991**, *37*, 1009.

(48) Huang, K. *Statistical Mechanics*, 2nd ed.; John Wiley: New York, 1987.

(49) Martys, N. S.; Shan, X.; Chen, H. Evaluation of the external force term in the discrete Boltzmann equation. *Phys. Rev. E* **1998**, *58*, 6855.

(50) He, X.; Luo, L.-S. Theory of the lattice Boltzmann method: From the Boltzmann equation to the lattice Boltzmann equation. *Phys. Rev. E* **1997**, *56*, 6811.

(51) He, X.; Luo, L.-S. A priori derivation of the lattice Boltzmann equation. *Phys. Rev. E* **1997**, *55*, R6333.

(52) Shan, X.; He, X. *Phys. Rev. Lett.* **1998**, *80*, 65.

(53) Worthing, R. A.; Mozer, J.; Seeley, G. Stability of lattice Boltzmann methods in hydrodynamic regimes. *Phys. Rev. E* **1997**, *56*, 2243.

(54) Sterling, J. D.; Chen, J. Stability analysis of lattice Boltzmann methods. *J. Comput. Phys.* **1996**, *123*, 196.

(55) Gustafsson, B.; Kreiss, H.-O.; Oliger, J. *Time dependent problems and difference methods*; John Wiley: New York, 1995.

(56) Glasser, B. J.; Kevrekidis, I. G.; Sundaresan, S. One- and two-dimensional travelling wave solutions in gas-fluidized beds. *J. Fluid Mech.* **1996**, *306*, 183.

(57) Glasser, B. J.; Sundaresan, S.; Kevrekidis, I. G. From bubbles to clusters in fluidized beds. *Phys. Rev. Lett.* **1998**, *81*, 1849.

Received for review February 18, 2008
Revised manuscript received May 15, 2008
Accepted May 19, 2008

IE800283B